Nanotechnology

PAPER

Tailoring the capability of carbon nitride (C_3N) nanosheets toward hydrogen storage upon light transition metal decoration

To cite this article: Omar Faye *et al* 2019 *Nanotechnology* **30** 075404

IOP Publishing Nanotechnology
Nanotechnology 30 (2019) 075404 (12pp) https://doi.org/10.1088/1361-6528/aaf3ed

Tailoring the capability of carbon nitride (C_3N) nanosheets toward hydrogen storage upon light transition metal decoration

Omar Faye[1], Tanveer Hussain[2], Amir Karton[2] and Jerzy Szpunar[1]

[1] Department of Mechanical Engineering, College of Engineering, University of Saskatchewan, 57 Campus Drive, Saskatoon, Saskatchewan S7N 5A9, Canada
[2] School of Molecular Sciences, The University of Western Australia, Perth, WA 6009, Australia

E-mail: tanveer.hussain@uwa.edu.au

Received 12 September 2018, revised 9 November 2018
Accepted for publication 26 November 2018
Published 21 December 2018

Abstract

To nurture the full potential of hydrogen (H_2) as a clean energy carrier, its efficient storage under ambient conditions is of great importance. Owing to the potential of material-based H_2 storage as a promising option, we have employed here first principles density functional theory calculations to study the H_2 storage properties of recently synthesized C_3N monolayers. Despite possessing fascinating structural and mechanical properties C_3N monolayers weakly bind H_2 molecules. However, our van der Waals corrected simulations revealed that the binding properties of H_2 on C_3N could be enhanced considerably by suitable Sc and Ti doping. The stabilities of Sc and Ti dopants on a C_3N surface has been verified by means of reaction barrier calculations and *ab initio* molecular dynamics simulations. Upon doping with C_3N, the existence of partial positive charges on both Sc and Ti causes multiple H_2 molecules to bind to the dopants through electrostatic interactions with adsorption energies that are within an ideal range. A drastically high H_2 storage capacity of 9.0 wt% could be achieved with two-sided Sc/Ti doping that ensures the promise of C_3N as a high-capacity H_2 storage material.

Keywords: energy carrier, adsorption, DFT, charge transfer, storage capacity

(Some figures may appear in colour only in the online journal)

1. Introduction

To reduce the impacts of climate change and fossil fuel depletion, increasing attention and efforts have been focused on the development of alternative energy sources and energy storage devices. To solve these issues, different renewables and clean energy sources have been tested. Based on the literature much attention has been devoted to hydrogen (H_2) as the future energy carrier for mobile applications since it is abundant, renewable, possesses much higher energy density than gasoline, and is clean as its byproduct is only H_2O [1, 2]. However, to make the H_2 economy a reality, we have to design safer and more efficient H_2 storage materials. In other words, to engineer an environmentally friendly material which could absorb H_2 molecules with at least 5.5 wt% of gravimetric density [3] and 30 g L^{-1} volumetric density, but release the stored H_2 under ambient conditions if needed, according to the US Department of Energy (US DOE). Furthermore, H_2 adsorption energy for an ideal material should be in the energy window of 0.1–0.8 eV [1].

In recent years, various classes of materials such as carbon nanotubes [4, 5], graphene [6–8], metal hydrides [9, 10], metal-organic frameworks [11, 12], graphane [13], graphdiyne [14] carbon nitride [15], and silanes [16] have been studied for H_2 storage applications. However, the main bottleneck of these materials in their pristine form is that H_2 binds weakly on their surfaces with a binding energy in the meV range, which causes H_2 desorption at very low temperatures [17]. In contrast, metal hydride shows a different behavior where H_2 molecules dissociates into H atoms, migrate into the material, and bind chemically with a binding energy in 2–4 eV range [1]. When the bonding is strong,

desorption of H_2 takes place at very higher temperatures [18]. To have an ideal case for H_2 storage under ambient conditions, the binding of H_2 with the above-mentioned materials must be improved through doping with foreign elements, for example transition metals (TMs), as reported by Cabria *et al* [19] and Yun *et al* [20] Earlier, we also predicted that Pd atom functionalized graphene [6] can absorb up to $4H_2$ molecules in the quasi-molecular form, which is the ideal interaction [1]. Yildirim and co-workers [21] also found that Ti-decorated carbon nanotubes could attain H_2 storage capacity of up to 8 wt% at ambient conditions.

On the chemical storage side, Liang *et al* [22] explained through mechanical milling how to make MgH_2-M (M = Ti, V, Mn, Fe, Ni) nanocomposite powders for H_2 storage. They found that the 3d elements revealed a different catalytic effect in the kinetic of the reaction and the desorption mechanism was enhanced at low temperatures. Similarly, Hussain *et al* [23] conducted a theoretical study on MgH_2 functionalized by TMs (Sc, V, Fe, Co, Ni, Cu, Y, Zr, and Nb). They reported that doping with TMs can enhance desorption of H_2 from MgH_2 at much lower temperature as compared to their pure forms. It has also been demonstrated by Yahya *et al* [24] that MgH_2 doped with 10 wt% of K_2NbF_7 and 5 wt% of multi-walled carbon nanotube, using the ball milling method, showed a significantly reduced decomposition temperature of 248 °C with a storage capacity of 6.2 wt%. The composite is able to absorb 5.2 wt% of H_2 at 150 °C in 60 min. In addition, 6 wt% of H_2 is released at 320 °C and 1 atm.

It is well understood that functionalized 2D materials offer a promising route to store H_2. Sheng *et al* [25] predicted that Li-Na decorated silicone could enhance H_2 storage capacity of higher than 6.5 wt% with a desirable binding energy of 0.29 eV/H_2. Yadav *et al* [8] reported that a single Zr atom attached on graphene surface can adsorb a maximum of $9H_2$ molecules with a binding energy of 0.34 eV/H_2 and an average desorption temperature of 433 K leading to a storage capacity of 11 wt%, higher than the DOE requirement of 5.5 wt%. Cabria *et al* [19] stated that the physisorption of H_2 on Li-doped graphene and nanotubes are about two times larger than on pure graphene and nanotubes. Zhou *et al* [26] reported that at a hydrogen charging pressure of 50 bar, the material could yield a gravimetric density of 6.7 wt% in 1% Pd/graphene nanocomposite. They also stated that by increasing the applied pressure to 60 bar, the hydrogen uptake capacity reached 8.67 wt% in the 1% Pd/graphene nanocomposite and 7.16 wt% in the 5% Pd/graphene nanocomposite [26].

Recently, a graphene-like 2D material called 2D polyaniline has been synthesized, which consists of three phenyl rings sharing six nitrogen atoms with the empirical formula of C_3N. It is a promising addition to the family of 2D materials due to its fascinating chemical, physical, and mechanical properties, which are quite distinctive from their original 3D bulk crystals [27–29]. Wang *et al* [30] stated that both the electron and hole mobilities are considerably high, for example, the hole mobility along the armchair direction of single-layer C_3N sheets can reach as high as $1.08 \times 10^4\ cm^2\ V^{-1}\ s^{-1}$. In addition, Makaremi *et al* [31] studied the adsorption of metallic, metalloid, and nonmetallic adatoms on C_3N monolayer. They found that the functionalization with nonmetallic and semi-metallic elements leads to a p-type doping and induces metallic behavior to the monolayer. They also reported that Si and Ge dopants can narrow the bandgap of carbon nitrides about 0.5–1.0 eV and also increase their optical absorption in the visible spectrum [32]. Furthermore, Javeed *et al* [33] described the synthesis of 2D polyaniline (C_3N) via the direct pyrolysis of hexaaminobenzene trihydrochloride single crystals in solid state. They further stated that doping of C_3N by hydrochloric acid, the conductivity of the latter jumped to almost 1960 times ($1.41 \times 10^3\ S\ cm^{-1}$) [33]. Moreover, Gao *et al* [34] stated that their density functional theory (DFT) result reveals that the lattice thermal conductivity of C_3N is as high as $380\ W\ mK^{-1}$, although much lower than that of graphene. Also, Li *et al* [35] stated that the unsaturated of zigzag C_3N nanoribbons are predicted to be magnetic metals or magnetic nearly half-metals depending on the ribbon width. Furthermore, Yang *et al* [36] reported large-scale synthesis of C_3N, a 2D crystalline, hole-free extension of graphene, its structural characterization, and some of its unique properties. In addition, C_3N is fabricated by polymerization of 2,3-diaminophenazine [36]. Based on its structure, mechanical, and electronic properties, C_3N monolayer could open up promising avenues in the field of H_2 storage. To the best of our knowledge, there are no experimental or theoretical investigations on H_2 storage on C_3N monolayer.

In this work, we have performed a comprehensive study based on first principles DFT to investigate the structural and H_2 storage properties of C_3N doped with scandium (Sc) and titanium (Ti). First, we study the favorable adsorption sites of these TMs and the electronic structure of the complex they form upon adsorption. Next, the clustering effect will be hurdles by studying the diffusion of Ti and Sc atoms on a C_3N monolayer. In addition, the stability of Sc@C_3N and Ti@C_3N complex will be further verified through *ab initio* molecular dynamics (AIMD) simulations. Finally, the binding mechanism of H_2 storage and its maximum storage capacity of Sc@C_3N and Ti@C_3N will be presented.

2. Computational approach

All calculations were carried out by means of DFT as implemented in DMol [3] codes with the atomic orbitals developed by Delley as the basis sets [37, 38]. To obtain reliable results, a careful selection of the exchange and correlation term to the total energy was crucial. According to Zupan *et al* [39] and Grossman *et al* [40] the local density approximation yielded overestimates of energy for molecular conformations or the crystal bulk phase. Nevertheless, the generalized gradient approximations (GGA) overcomes these deficiencies and produces a more realistic description of energy barriers in the dissociative adsorption of H_2 on metal and semiconductor surfaces [41–43]. Therefore, to evaluate the exchange-correlation interaction we have used GGA [43, 44] with the Perdew–Wang 91 functional [45] throughout

this paper. The DFT semi-core pseudopotentials used as the core treatment with double numerical basis set (DNP) augmented with p-polarization function is applied, in which Ti: $3s^2\ 3p^6\ 3d^2\ 4s^2$, Sc: $3s^2\ 3p^6\ 3d^1\ 4s^2$, C:$2s^2\ 2p^2$, and H:$1s^1$ states are treated as valence electrons. Spin-polarization was allowed in all calculations. To improve the weak interaction in a neutral system, DFT-D correction was applied to include the van der Waals (vdW) interaction by applying the Ortmann, Bechstedt, and Schmidt [46] scheme, which added a contribution of $\frac{\epsilon}{R^{-6}}$ in the DFT total energy for a pairwise interaction separated by R. To model our system we used a 2×2 supercell consisting of two types of hexagonal rings, the CC rings with six carbon atoms and the NC rings with two nitrogen and four carbon atoms. The periodic boundary condition was used along the x and y directions. The Brillouin zone integration was performed through the Monkhorst−Pack scheme [47] with a mesh grid of $13 \times 13 \times 1$. The lattice parameters of the optimized supercell were $a = b = 9.716$ and $c = 12.5$ Å. The energy minimization was performed with an energy convergence tolerance of 10^{-5} Ha. The atomic relation was done with the force convergence criterion of 0.002 Ha/Å. The diffusion of Sc and Ti on C_3N was studied by using transition state (TS) calculations based on the complete linear synchronous transit and quadratic synchronous transit methods [48]. The activation energy (E_a) and the reaction energy are defined as:

$$E_a = T_{(TS)} - E_{(R)} \quad (1)$$

$$E_{reaction} = E_P - E_R, \quad (2)$$

where $T_{(TS)}$ is the energy of the transition state in each elementary reaction, $E_{(R)}$ is the energy of the reactant in each reaction, and E_P is the energy of the product in each reaction.

3. Results and discussion

3.1. Electronic structure of Sc- and Ti-doped C_3N

Before studying the functionalization of both Sc and Ti on C_3N nanosheets, we will describe the structural properties of C_3N bulk, the corresponding lattice parameter, and bond lengths. We found that the lattice parameter of bulk C_3N is $a = b = 4.858$ Å, C–C and C–N bond lengths are 1.400 Å and 1.397 Å, respectively compared to $a = b = 4.861$ Å, and C–C = C–N = 1.40 Å as reported by Makaremi *et al* [31]. These results validated the level of theory being employed in this work. Furthermore, to study the interaction of Sc and Ti dopants on a C_3N sheet, a 2×2 supercell of C_3N is considered as shown figure 1, which displays that C_3N has two types of hexagonal rings as mentioned above. In addition, each ring has three high symmetry points, namely, hollow (H), top (T), and bridge (B) as depicted in figure 1.

The interaction of Sc with C_3N (Sc@C_3N) and Ti with C_3N (Ti@C_3N) is carried out on its high symmetry points. The adsorption energies have been calculated by the following equation (3):

$$E_{ads} = -(E_{AB} - E_A - E_B), \quad (3)$$

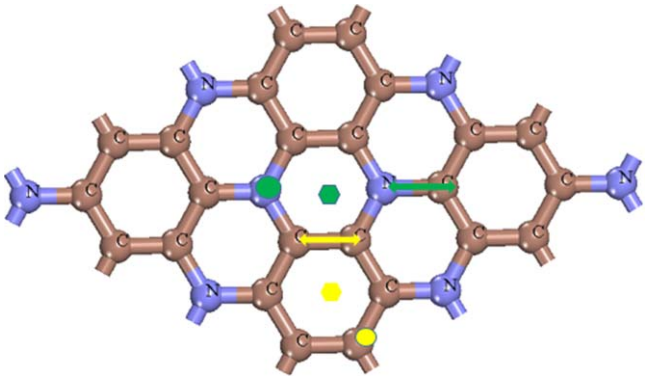

Figure 1. Optimized structures of $2 \times 2 \times 1$ supercell of C_3N with the two rings and their three high symmetry points. Brown and blue balls represent C and N atoms, respectively.

where E_{AB} is the total energy of the complex formed after adsorption (Sc@C_3N and Ti@C_3N), E_A is the total energy of the C_3N monolayer, and E_B is the total energy of each dopant (Sc and Ti). The most favorable adsorption site for Sc and Ti dopants has been summarized and compared with the results available in the literature as shown in table 1. We found that the most favorable adsorption site for Sc and Ti in C_3N is the hollow (H) site of the CC rings with six carbon atoms. The corresponding E_{ads} are 3.745 and 4.161 eV for Si@C_3N and Ti@C_3N, respectively which are close to their experimental bulk cohesive energies of 3.90 eV for Sc and 4.85 eV for Ti as reported by Philipsen *et al* [49] In addition, Makaremi *et al* [31] reported that the binding energies of Sc and Ti on C_3N are 1.84 and 2.25 eV, respectively, which are lower than our calculated values. Furthermore, Durgun *et al* [50] predicted that the most stable adsorption sites for Sc and Ti on graphene sheet is the H site with a binding energy of 1.59 and 1.22 eV, respectively, which are lower than 2.08 and 3.27 eV for Sc and Ti-decorated graphene [51]. The slight difference in the E_{ads} values may be due to the choice of the functional. Makaremi *et al* [31] used the Perdew−Burke−Ernzerhof functional compared to the Perdew–Wang 91 functional in this work. Thus, our results show a good agreement with earlier results reported in the literature. Moreover, we have computed the E_{ads} in the NC rings with two nitrogen and four carbon atoms. We found that Sc and Ti prefer to bind above the nitrogen atom (top position) with E_{ads} of 3.50 and 3.87 eV, respectively. While in the H site of the NC ring the E_{ads} of Sc and Ti dopants are 3.283 and 3.566 eV, respectively.

We have studied the electronic properties of pristine and Sc/Ti-decorated C_3N monolayers. On this end we found that C_3N is a semiconductor with a bandgap (E_g) of 0.457 eV compared to 2.67 [33], 0.405 [52], and 1.09 eV [53]. Furthermore, the functionalization of Sc and Ti dopants on the C_3N surface caused a reduction in the E_g to 0.425 eV for Sc and 0.3120 eV for Ti.

To understand the charge transfer mechanism, we employed Mulliken population analysis. This analysis revealed that C–N is a polar covalent bond with −0.410e for the N atom and 0.137e for the C atom compared to −0.34e for the N atom

Table 1. Adsorption energy for the most favorable adsorption site of Ti and Sc atoms along with some results from the literature.

System	Adsorption site	Binding energy (eV)	Reference [27]	Reference [43]	Reference [44]
Sc+C_3N	H_{CC}	3.745	1.84	1.59 eV	2.08
Ti+C_3N	H_{CC}	4.161	2.25	1.22	3.27

and 0.110e for the C atom according to Shi *et al* [53] The charge transfer from Ti to C_3N is 0.604e, which is higher than the value of 0.520e in the case of Sc to C_3N. In addition, we calculated the isosurface charge density by using the equation (4)

$$\Delta\rho = \rho(C_3N@Sc/Ti) - \rho(C_3N) - \rho(Sc/Ti). \quad (4)$$

Isosurface plots for Sc- and Ti-decorated C_3N are given in figure 2.

The clustering of metal dopants on the monolayers is a drawback for hydrogen storage, especially in the case of TMs with higher cohesive energies. Therefore, it is important to investigate this issue for the studied systems (Sc@C_3N and Ti@C_3N) before testing them as an H_2 storage medium. To this end, we calculated the diffusion paths of both Sc and Ti on C_3N using TS calculation. Figure 3 summarizes the possible diffusion paths of Sc and Ti on the C_3N surface. Two possible diffusion paths have been investigated on the C_3N surface as shown in figure 3. The calculated energy barrier is 0.666 eV for the diffusion of Ti from the H site of the CC ring to the top of the N atom of the NC ring and 0.416 eV for Sc for the same path and their corresponding energy of reaction are 0.245 and 0.291 eV, respectively. While the second route, which is the migration from the H site of the CC ring to the H site of the NC ring, requires an activation energy of 0.625 and 0.483 eV for Ti and Sc, respectively. The reaction energy during this process is 0.462 eV for Sc and 0.595 eV for Ti. These results show that the diffusion path from the H site of the CC ring to the H site of the NC ring is most favorable for the Ti atom, while the migration path of the Sc atom from the H site of the CC ring to the T site on the N atom of the NC ring is the most favorable one. The high-energy barrier of Ti@C_3N and Sc@C_3N compared to their thermal vibration at room temperature ($T = 300$ K) is 0.03 eV, suggesting that Ti@C_3N and Sc@C_3N are stable at $T = 300$ K. Therefore, one can conclude that both the Sc and Ti atoms are stable on C_3N monolayers at normal temperature. In addition, the stability of Sc- and Ti-decorated C_3N monolayers has been further verified through AIMD at 300 K and 800 K in order to evaluate the strength of the thermal vibration. For this purpose we have employed the Nose Thermostat algorithm for 6 ps on Sc@C_3N and Ti@C_3N and the results at $T = 300$ K and $T = 800$ K are plotted in figures 4 and 5, respectively. A small change in the energy for both systems supplements their thermodynamic stabilities. Base on the equipartition theorem the average thermal energy of a molecule in three-dimensional space is given by

$$E_{avg} = \frac{3K_BT}{2}, \quad (5)$$

where K_B = the Boltzmann constant ($8.617\,3310^{-5}$ eV /K) and T = temperature in Kelvin. Since Ti and Sc atoms vibrate

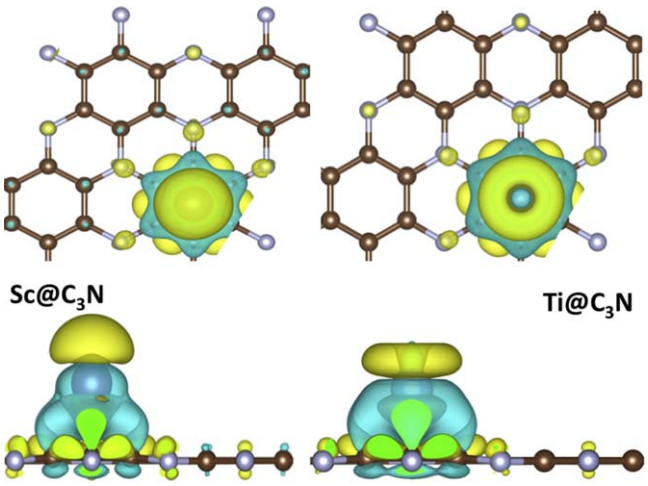

Figure 2. Top and side views of isosurface charge densities of Sc@C_3N and Ti@C_3N. Yellow and cyan colors represent depletion and accumulation of charges. The isovalue is taken as 0.005 e/Å^3.

in the plane equation (5) turns out to be $E_{avg} = K_BT$. Therefore, the thermal vibration energy at $T = 300$ K is found to be 0.025 and 0.069 eV at $T = 800$ K which are very small compared to 0.416 eV, 0.480 eV as the energy barrier for the Ti atom, and 0.666 and 0.625 eV for the Sc atom. In conclusion, the small value of the vibration energy of the Ti and Sc atoms at $T = 300$ K and $T = 800$ K compared to their high-energy barriers showed that the clustering of Ti and Sc atoms on the C_3N plane is not favorable. Therefore, in the next section we will explore Ti@C_3N and Sc@C_3N systems as hydrogen storage media.

3.2. Hydrogen uptake of TMs-doped C_3N (TMs = Sc, Ti)

In this section, the successive addition of an H_2 molecule on Sc@C_3N and Ti@C_3N has been investigated. The adsorption energies of Sc@C_3N and Ti@C_3N along with their equilibrium parameters are summarized in table 2. The first H_2 interacts with Ti@C_3N and Sc@C_3N leads to an E_{ads} of 0.422 and 0.221 eV, respectively, which are in close agreement with that of metal decorated polyacetylene [54]. Durgun *et al* [50] reported the E_{ads} of H_2 on Ti- and Sc-decorated graphene is 0.35 and 0.17 eV, respectively. We observed a stretching of the H_2 bond length from 0.750 Å–0.831 Å for Ti@C_3N compared to 0.806 Å for Sc@C_3N. The average distance between the H atom and the TM dopants are 1.959 Å for Ti@C_3N and 2.13 Å in the case of Sc@C_3N. The elongation of H–H bonds are consistent with the Kubas-type of interaction, which is electron donation between the metal and the H_2 molecule for an empty d orbital [55]. We predict that Ti@C_3N and Sc@C_3N complexes could bind up to five H_2 in the quasi-molecular form as depicted in figure 6. The

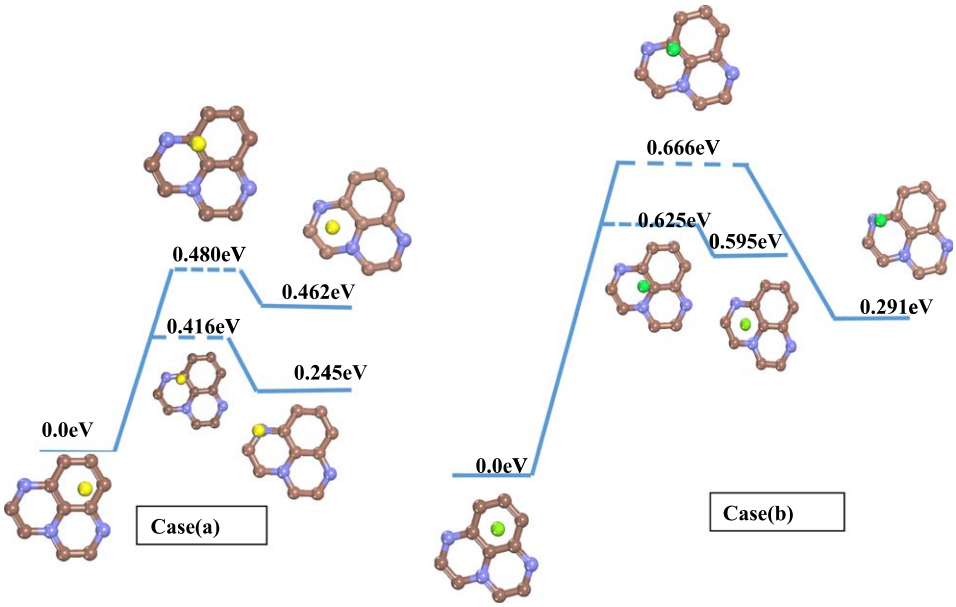

Figure 3. The potential energy of Ti and Sc atoms on C_3N. Case (a) corresponds to the Sc atom and (b) for the Ti atom. The brown, blue, yellow, and green balls represent C, N, Sc, and Ti atoms, respectively.

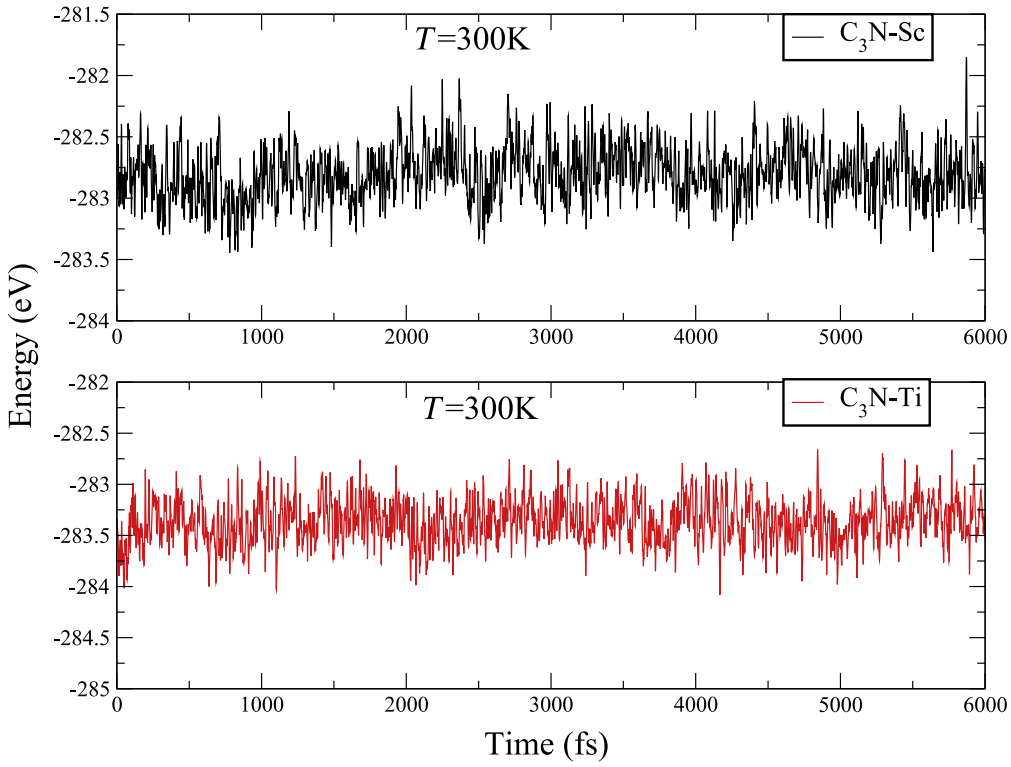

Figure 4. Variation in energies versus time steps for Sc/Ti-decorated C_3N monolayers at $T = 300$ K.

adsorption of an additional H_2 leads to a metastable configuration. These results agree well with earlier works [50, 51, 54].

To better understand the binding mechanism of H_2 on Ti@C_3N and Sc@C_3N complexes we plotted the equilibrium parameters (average adsorption energy (E_{ads}), H–H bond length, and TMs–H distance) of these systems in figure 7. We noted a significant increase of the E_{ads} for the first $3H_2$ molecules adsorbed on Ti@C_3N ranging from 0.422–0.725 eV, which slowly decreased to a minimum value of 0.555 eV for the sixth H_2 adsorption corresponding to the metastable configuration as illustrated in figure 7(a). The elongation of the H–H bond reached its maximum value 0.856 Å for the first $2H_2$ molecule and decreased gradually to a minimum of 0.793 Å for the adsorption of the sixth H_2 molecule as depicted in figure 7(b). The distance between the Ti and H atoms (Ti–H) oscillates in the interval of 1.875 Å–1.959 Å for the first $4H_2$ on Ti@C_3N and gradually increased for the last two addition of H_2 to a value 2.310 Å as shown figure 7(c). The calculated energy gap for the

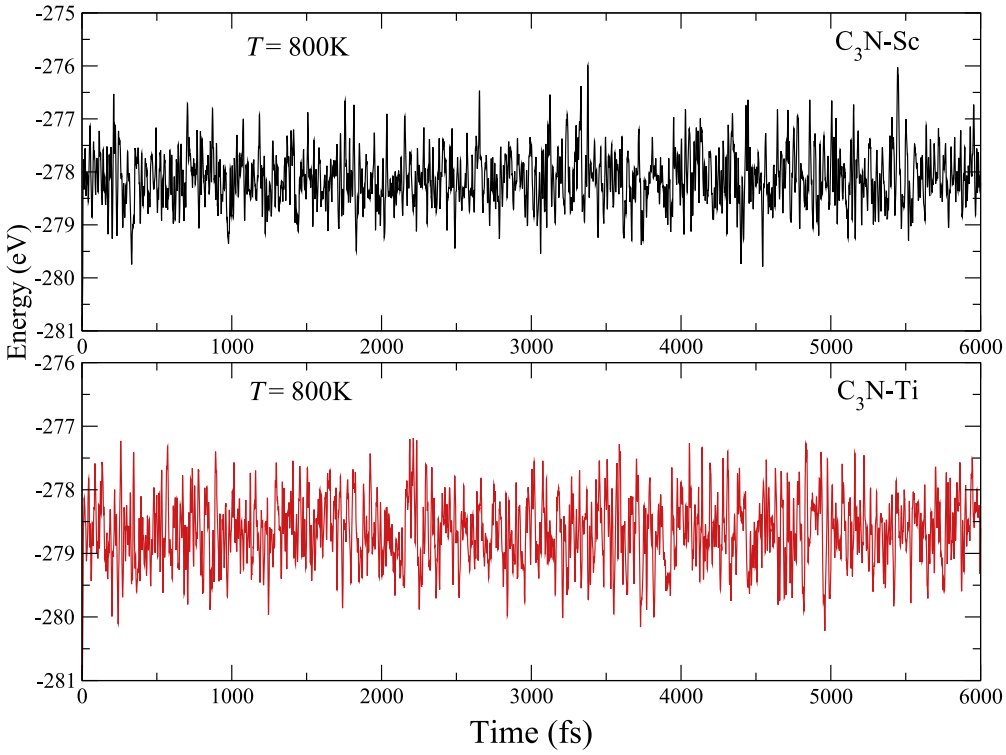

Figure 5. Snapshots of molecular dynamics (MD) simulations of $Sc@C_3N$ and $Ti@C_3N$ at $T = 800$ K.

Table 2. The E_{ads} of H_2 on $Sc@C_3N$ and $Ti@C_3N$, H–H bond lengths, TMs–H bond lengths and bandgaps.

nH_2+Ti@C_3N	Number of H_2	E_{ads} (eV)	H–H (Å)	Ti–H (Å)	E_g (eV)	Td (K)
	1	0.422	0.831	1.959	0.323	312
	2	0.670	0.856	1.875	0.988	496
	3	0.725	0.838	1.881	1	536
	4	0.661	0.815	1.932	0.792	489
	5	0.585	0.801	2.056	0.803	433
	6	0.555	0.793	2.310	0.784	410
nH_2+Sc@C_3N	1	0.221	0.806	2.13	0.530	163
	2	0.415	0.831	2.031	0.862	307
	3	0.507	0.820	2.032	1.034	375
	4	0.528	0.805	2.058	0.888	390
	5	0.481	0.795	2.207	0.890	356
	6	0.462	0.786	2.441	0.906	342

first $3H_2$ increases from 0.323–1 eV, and then decreased slowly to 0.784 eV as represented in figure 7(d). These results showed that the addition of H_2 affects the bandgap of the $Ti@C_3N$ complex.

In figure 8, we present the variation of the binding energies with respect to the number of H_2 for $Sc@C_3N$. From figure 8(a), we observed a sharp increase in the first addition of $4H_2$ on $Sc@C_3N$ from 0.221–0.528 eV, which then decreased gradually to a minimum value of 0.462 eV for the sixth addition of H_2. The first $2H_2$ molecules increased from 0.806–0.831 Å and slowly decreased to a minimum value of 0.786 Å. Figure 8(c) represents the variation in Sc–H distance as a function of the number of H_2, due to strong interaction of the first $4H_2$ molecules on $Sc@C_3N$; we noted a slight fluctuation of Sc–H distance in the window of 2.031 Å–2.13 Å and an increase to 2.441 Å for the sixth addition of H_2. The changes in the energy gap (E_g) with the number of H_2 is also plotted in figure 8(d), where we note a stiff increase in the bandgap for the first $3H_2$ from 0.530–1.034 eV and a fluctuation between 0.888 and 0.906 eV. These results showed that the addition of H_2 molecule affected the physical properties of the $Ti@C_3N$ and $Sc@C_3N$ complex.

Moreover, we used the van't Hoff equation as given below to derive the desorption temperature (T_D) of the H_2 molecule from the $Ti@C_3N$ and $Sc@C_3N$ complexes. The relation between the equilibrium constant and the thermodynamic quantities are given as

$$\ln K_{eq} = \left(-\frac{\Delta H}{RT} + \frac{\Delta S}{R}\right), \tag{6}$$

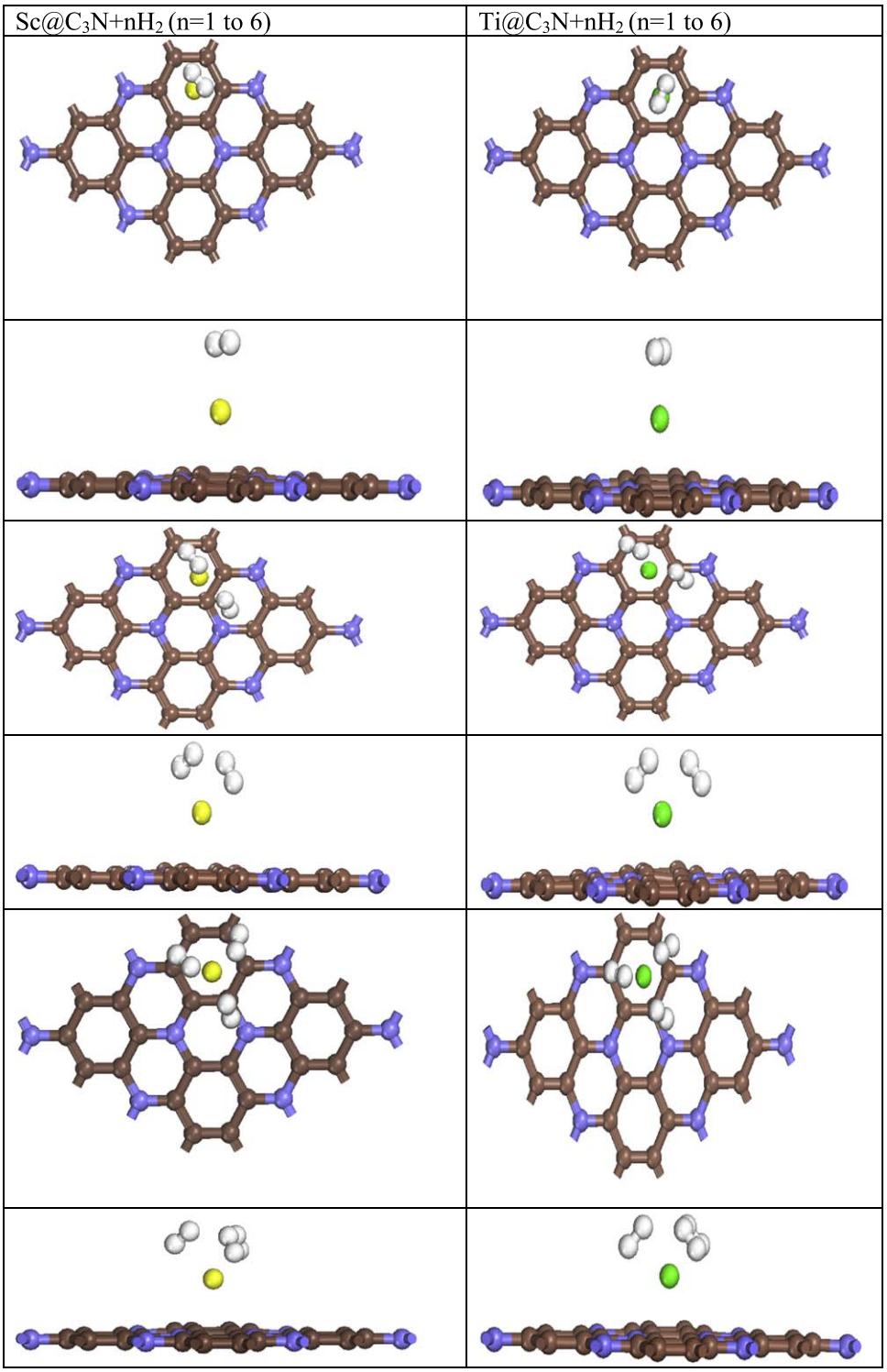

Figure 6. Optimized structures of $Sc@C_3N$ and $Ti@C_3N$ saturated with nH_2 molecules. The brown, blue, green, yellow and white balls represent C, N, Sc, Ti, and H atoms, respectively.

where $K_{eq} = \frac{P_{H_2}}{P_0}$, P_{H_2} and P_0 are equilibrium and reference pressure (atmospheric pressure) respectively, R is the universal gas constant, T is the absolute temperature, ΔH is the change in H_2 enthalpy, and ΔS is the change in H_2 entropy from gas to condensed phase.

By rearranging the van't Hoff equation we can evaluate the desorption temperature T_D as

$$T_D = \left(\frac{E_{ads}}{K_B}\right)\left(\frac{\Delta S}{R} - \ln\left(\frac{P}{P_0}\right)\right)^{-1}, \quad (7)$$

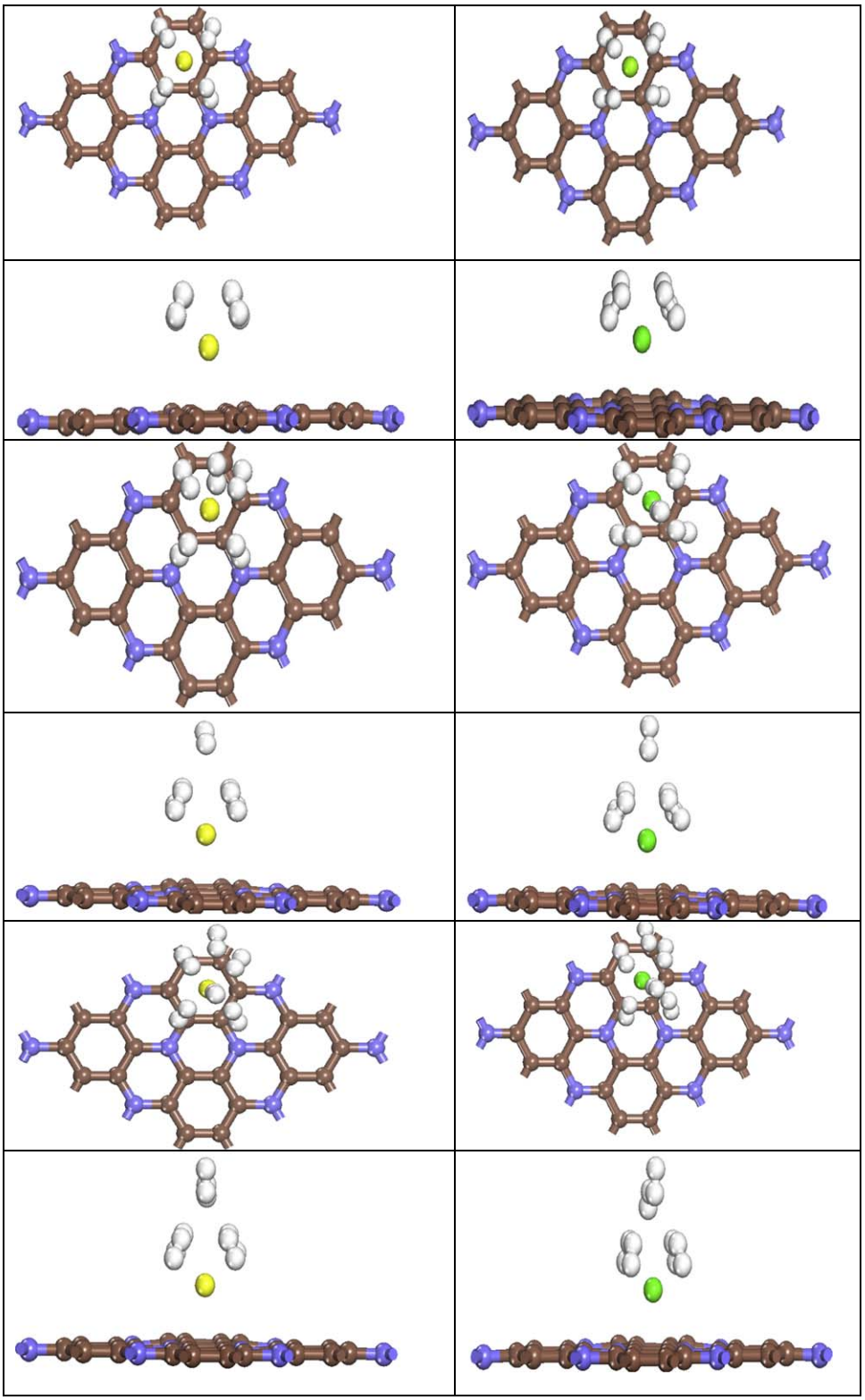

Figure 6. (Continued.)

where $E_{ads} = \frac{\Delta H}{N}$, the adsorption energy, K_B is the Boltzmann constant, $P = 1$ atm, R the universal gas constant, and $\Delta S = 130.7\,J.\,K^{-1}\,mol^{-1}$ is the change in H_2 entropy [56–58]. For successive H_2 addition on the $Ti@C_3N$ and $Sc@C_3N$ complexes. In figure 9, we plotted the desorption temperature as a function of the average binding energy as shown in figure 9(a) and figure 8(b) for $nH_2 + Sc@C_3N$ and $nH_2 + Ti@C_3N$, respectively, but also as a function of the number (n) of H_2 molecules absorbed as shown in figures 9(c) and (d). We observed a linear change in the average desorption temperature

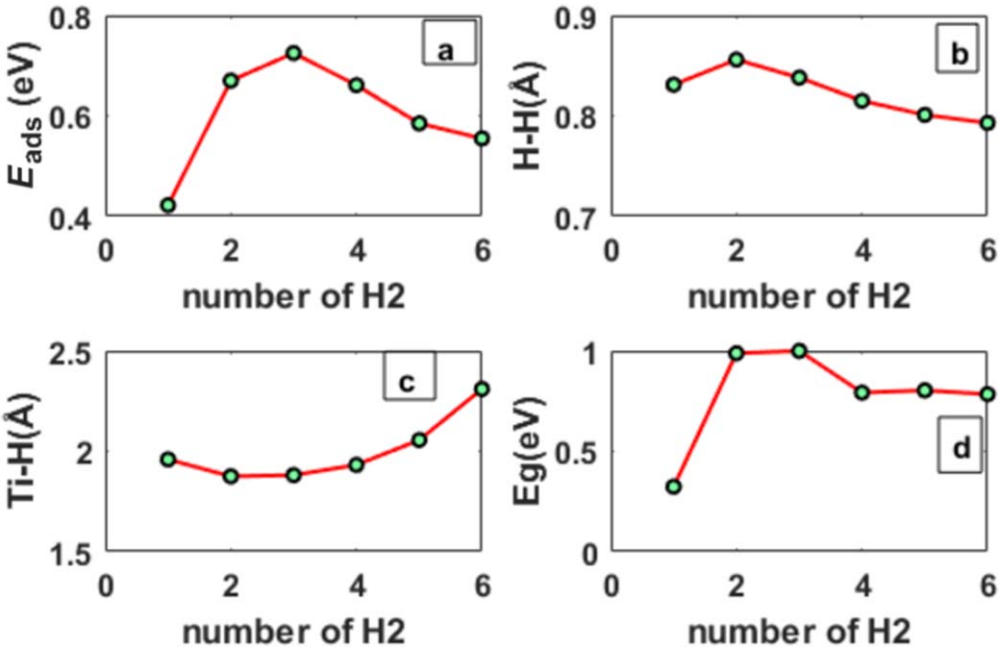

Figure 7. Physical and chemical parameters of the successive adsorption of H_2 on Ti@C_3N. Case (a) corresponds to the variation of the binding energy with respect to the number of H_2 molecules, (b) represents the variation of H–H with the number of H_2 molecules, (c) the changes in Ti–H with respect to the number of H_2, and (d) the variation of E_g with the number of H_2 molecules.

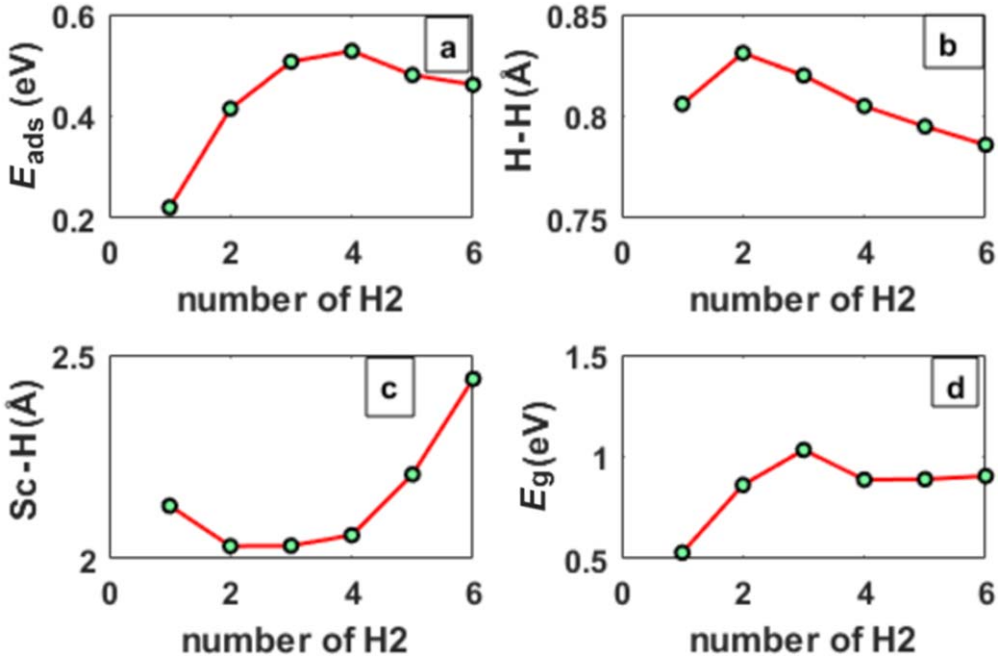

Figure 8. Physical and chemical parameters of the successive addition of H_2 on Sc@C_3N. Case (a) corresponds to the variation of the binding energy with respect to the number of H_2 molecules, (b) represents the variation of H–H with the number of H_2 molecules, (c) the changes of Ti–H with respect the number of H_2, and (d) the variation of E_g with the number of H_2 molecules.

as a function of the average binding energy as depicted in figure 9(a) and figure 9(b) for nH_2 + Sc@C_3N and nH_2 + Ti@C_3N, respectively. To better visualize the maximum average temperature requires the desorption of all the H_2 molecules from Sc@C_3N and Ti@C_3N, and we plotted the average desorption temperature as a function of the number of H_2 molecules in figures 9(c) and (d). We learned that the maximum average temperature requires the desorption of the complex $6H_2$ + Ti@C_3N and is $T_{dmax} = 536$ K compared to $T_{dmax} = 390$ K for the complex $6H_2$ + Sc@C_3N. We also note that the onset desorption temperature is $T_{dmin} = 312$ K for nH_2 + Ti@C_3N and $T_{dmin} = 160$ K for the nH_2 + Sc@C_3N

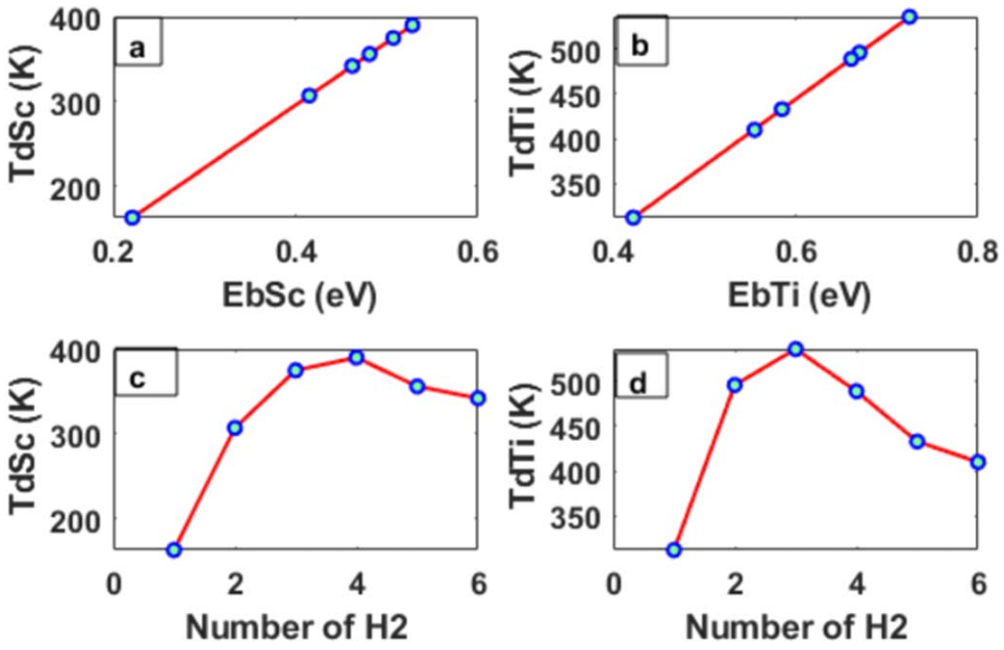

Figure 9. Represents the desorption temperature of H_2 molecules from the complexes (a) Sc@C_3N, (b) Ti@C_3N as a function of their binding energy and (c) and (d) as the number of desorbed H_2 molecules.

system. In addition, we use equation (8) to evaluate the weight percent of the H_2 molecules in our systems.

$$H_2(\text{wt}\%) = \left[\frac{M_{H2}}{M_{H2} + M_{\text{host}}}\right] \times 100, \qquad (8)$$

where M_{H2} represents the mass of the total number of H_2 molecules adsorbed and M_{host} refers to the mass of the sorbent.

Furthermore, the H_2 storage capacity by functionalizing C_3N on both sides by Sc and Ti dopants, which means two dopants on C_3N, can be deduced. Since each dopant can adsorb five H_2 molecules this means that C_3N functionalized on both sides of Sc and Ti can adsorb $10H_2$. Therefore, using equation (8) one can predict that the H_2 storage capacity for Ti@C_3N and Sc@C_3N is higher than 9.0 wt%, due to the fact that each system can adsorb $10H_2$ molecules, which is much higher than the DOE target. Even though Ti@C_3N has a storage capacity higher than 9 wt% like Sc@C_3N, based on our results Sc@C_3N is thermodynamically more promising for H_2 storage than the Ti@C_3N system.

4. Conclusion

To conclude, we have employed rigorous first principles calculations based on DFT to study the structural, electronic, and H_2 storage properties of Sc/Ti-decorated novel two-dimensional C_3N monolayers. Reasonably high binding energies and large diffusion barriers restrict the dopants (Sc, Ti) from clustering over C_3N surfaces. The stabilities of doped systems have been further verified by performing MD simulations at 300 K and 800 K for 6 ps and the systems remained stable. Charge transfer analysis indicated the presence of partial positive charges on Sc/Ti upon their binding with C_3N. We have found that each Sc@C_3N and Ti@C_3N anchor multiple H_2 molecules attaining a high storage capacity of 9 wt%, easily exceeding the DOE target. The vdW-corrected H_2 adsorption energies fall in the ideal range to ensure the promise of Sc/Ti-decorated C_3N monolayers as efficient H_2 storage materials for mobile applications.

Acknowledgments

The National Engineering Research Council of Canada and the Canada Research Chair program supported this work. TH acknowledges the resources at the NCI National Facility systems at the Australian National University through the National Computational Merit Allocation Scheme supported by the Australian Government. AK acknowledges an Australian Research Council (ARC) Future Fellowship (FT170100373).

Notes

The authors declare no competing financial interest.

ORCID iDs

Tanveer Hussain https://orcid.org/0000-0002-0300-0503

References

[1] Jena P 2011 Materials for hydrogen storage: past, present, and future *J. Phys. Chem. Lett.* **2** 206–11
[2] Hussain T, De Sarkar A and Ahuja R 2014 Functionalization of hydrogenated graphene by polylithiated species for efficient hydrogen storage *Int. J. Hydrogen Energy* **39** 2560–6

[3] Suh M P, Park H J, Prasad T K and Lim D-W 2011 Hydrogen storage in metal–organic frameworks *Chem. Rev.* **112** 782–835

[4] Tada K, Furuya S and Watanabe K 2001 *Ab initio* study of hydrogen adsorption to single-walled carbon nanotubes *Phys. Rev.* B **63** 155405

[5] Dag S, Ozturk Y, Ciraci S and Yildirim T 2005 Adsorption and dissociation of hydrogen molecules on bare and functionalized carbon nanotubes *Phys. Rev.* B **72** 155404

[6] Faye O, Szpunar J A, Szpunar B and Beye A C 2017 Hydrogen adsorption and storage on palladium–functionalized graphene with NH-dopant: a first principles calculation *Appl. Surf. Sci.* **392** 362–74

[7] Faye O, Eduok U, Szpunar J, Szpunar B, Samoura A and Beye A 2017 Hydrogen storage on bare Cu atom and Cu-functionalized boron-doped graphene: a first principles study *Int. J. Hydrogen Energy* **42** 4233–43

[8] Yadav A, Chakraborty B, Gangan A, Patel N, Press M R and Ramaniah L M 2017 Magnetic moment controlling desorption temperature in hydrogen storage: a case of zirconium-doped graphene as a high capacity hydrogen storage medium *J. Phys. Chem.* C **121** 16721–30

[9] German E and Gebauer R 2016 Improvement of hydrogen vacancy diffusion kinetics in MgH_2 by niobium-and zirconium-doping for hydrogen storage applications *J. Phys. Chem.* C **120** 4806–12

[10] Schlapbach L and Züttel A 2011 Hydrogen-storage materials for mobile applications *Materials for Sustainable Energy: A Collection of Peer-Reviewed Research and Review Articles from Nature Publishing Group* (Singapore: World Scientific) pp 265–70

[11] Deshmukh A, Le T N M, Chiu C-C and Kuo J-L 2018 DFT study on the H2 storage properties of Sc-decorated covalent organic frameworks based on adamantane units *J. Phys. Chem.* C **122** 16853–65

[12] Kumar S, Samolia M and Dhilip Kumar T J 2018 Hydrogen storage in Sc and Li decorated metal–inorganic framework *ACS Appl. Energy. Mater.* **1** 1328–36

[13] Hussain T, Pathak B, Maark T A, Araujo C M, Scheicher R H and Ahuja R 2011 *Ab initio* study of lithium-doped graphane for hydrogen storage *EPL* **96** 27013

[14] Panigrahi P, Dhinakaran A, Naqvi S, Rao S G, Ahuja R and Hussain T 2018 Light metal decorated graphdiyne (Gdy) nanosheets for reversible hydrogen storage *Nanotechnology* **29** 355401

[15] Hussain T, Hankel M and Searles D J 2016 Computational evaluation of lithium-functionalized carbon nitride ($g\text{-}C_6N_8$) monolayer as an efficient hydrogen storage material *J. Phys. Chem.* C **120** 25180–8

[16] Ventura-Espinosa D, Sabater S, Carretero-Cerdán A, Baya M and Mata J A 2018 High production of hydrogen on demand from silanes catalyzed by iridium complexes as a versatile hydrogen storage system *ACS. Catal.* **8** 2558–66

[17] Yürüm Y, Taralp A and Veziroglu T N 2009 Storage of hydrogen in nanostructured carbon materials *Int. J. Hydrogen Energy* **34** 3784–98

[18] Bogdanović B, Bohmhammel K, Christ B, Reiser A, Schlichte K, Vehlen R and Wolf U 1999 Thermodynamic investigation of the magnesium–hydrogen system *J. Alloys Compd.* **282** 84–92

[19] Cabria I, López M and Alonso J 2005 Enhancement of hydrogen physisorption on graphene and carbon nanotubes by Li doping *J. Chem. Phys.* **123** 204721

[20] Liu Y, Brown C M, Neumann D A, Geohegan D B, Puretzky A A, Rouleau C M, Hu H, Styers-Barnett D, Krasnov P O and Yakobson B I 2012 Metal-assisted hydrogen storage on Pt-decorated single-walled carbon nanohorns *Carbon* **50** 4953–64

[21] Yildirim T, Íñiguez J and Ciraci S 2005 Molecular and dissociative adsorption of multiple hydrogen molecules on transition metal decorated C60 *Phys. Rev.* B **72** 153403

[22] Liang G, Huot J, Boily S, Van Neste A and Schulz R 1999 Catalytic effect of transition metals on hydrogen sorption in nanocrystalline ball milled MgH_2–Tm (Tm=Ti, V, Mn, Fe and Ni) systems *J. Alloys Compd.* **292** 247–52

[23] Hussain T, Maark T A, Chakraborty S and Ahuja R 2015 Improvement in hydrogen desorption from β-and γ-MgH_2 upon transition-metal doping *ChemPhysChem.* **16** 2557–61

[24] Yahya M S and Ismail M 2018 Improvement of hydrogen storage properties of MgH_2 catalysed by K2NbF7 and multiwall carbon nanotube *J. Phys. Chem.* C **122** 11222–33

[25] Sheng Z, Wu S, Dai X, Zhao T and Hao Y 2018 A first-principles study of hydrogen storage capacity based on Li–Na-decorated silicene *Phys. Chem. Chem. Phys.* **20** 13903–8

[26] Zhou C and Szpunar J A 2016 Hydrogen storage performance in Pd/graphene nanocomposites *ACS Appl. Mater. Interfaces* **8** 25933–40

[27] Geim A K and Grigorieva I V 2013 Van der Waals heterostructures *Nature* **499** 419

[28] Hong Y, Zhang J and Zeng X C 2018 Monolayer and bilayer polyaniline C_3N: two-dimensional semiconductors with high thermal conductivity *Nanoscale* **10** 4301–10

[29] Mortazavi B 2017 Ultra high stiffness and thermal conductivity of graphene like C_3N *Carbon* **118** 25–34

[30] Wang X, Li Q, Wang H, Gao Y, Hou J and Shao J 2018 Anisotropic carrier mobility in single-and bi-layer C_3N sheets *Physica* B **537** 314–9

[31] Makaremi M, Mortazavi B and Singh C V 2017 Adsorption of metallic, metalloidic, and nonmetallic adatoms on two-dimensional C_3N *J. Phys. Chem.* C **121** 18575–83

[32] Makaremi M, Grixti S, Butler K T, Ozin G A and Singh C V 2018 Band engineering of carbon nitride monolayers by N-type, P-type, and isoelectronic doping for photocatalytic applications *ACS Appl. Mater. Interfaces* **10** 11143–51

[33] Mahmood J, Lee E K, Jung M, Shin D, Choi H J, Seo J M, Jung S M, Kim D, Li F and Lah M S 2016 Two-dimensional polyaniline (C_3N) from carbonized organic single crystals in solid state *Proc. Natl Acad. Sci. USA* **113** 7414–9

[34] Gao Y, Wang H, Sun M, Ding Y, Zhang L and Li Q 2018 First-principles study of intrinsic phononic thermal transport in monolayer C_3N *Physica E: Low-dimensional Systems and Nanostructures* **99** 194–201

[35] Li Q, Wang H, Pan H and Ding Y 2018 Tunable electronic structures and magnetic properties of zigzag C_3N nanoribbons *J. Phys. D: Appl. Phys.* **51** 345301

[36] Yang S *et al* 2017 C3N—A 2D crystalline, hole-free, tunable-narrow-bandgap semiconductor with ferromagnetic properties *Adv. Mater.* **29** 1605625

[37] Delley B 2000 From molecules to solids with the $DMol^3$ approach *J. Chem. Phys.* **113** 7756–64

[38] Delley B 1990 An all-electron numerical method for solving the local density functional for polyatomic molecules *J. Chem. Phys.* **92** 508–17

[39] Zupan A, Blaha P, Schwarz K and Perdew J P 1998 Pressure-induced phase transitions in solid Si, SiO_2, and Fe: performance of local-spin-density and generalized-gradient-approximation density functionals *Phys. Rev.* B **58** 11266

[40] Grossman J C, Mitas L and Raghavachari K 1995 Structure and stability of molecular carbon: importance of electron correlation *Phys. Rev. Lett.* **75** 387

[41] Hammer B, Scheffler M, Jacobsen K W and Nørskov J K 1994 Multidimensional potential energy surface for H2 dissociation over Cu(111) *Phys. Rev. Lett.* **73** 1400

[42] Penev E, Kratzer P and Scheffler M 1999 Effect of the cluster size in modeling the H2 desorption and dissociative adsorption on Si(001) *J. Chem. Phys.* **110** 3986–94

[43] Burke K, Perdew J P and Wang Y 1998 Derivation of a generalized gradient approximation: the PW91 density functional *Electronic Density Functional Theory* (Berlin: Springer) pp 81–111
[44] Becke A D 1997 Density-functional thermochemistry. V. Systematic optimization of exchange-correlation functionals *J. Chem. Phys.* **107** 8554–60
[45] Okamoto Y and Miyamoto Y 2001 *Ab initio* investigation of physisorption of molecular hydrogen on planar and curved graphenes *J. Phys. Chem.* B **105** 3470–4
[46] Ortmann F, Bechstedt F and Schmidt W 2006 Semiempirical van der Waals correction to the density functional description of solids and molecular structures *Phys. Rev.* B **73** 205101
[47] Monkhorst H J and Pack J D 1976 Special points for Brillouin-zone integrations *Phys. Rev.* B **13** 5188
[48] Govind N, Petersen M, Fitzgerald G, King-Smith D and Andzelm J 2003 A generalized synchronous transit method for transition state location *Comput. Mater. Sci.* **28** 250–8
[49] Philipsen P H T and Baerends E J 1996 Cohesive energy of 3d transition metals: density functional theory atomic and bulk calculations *Phys. Rev.* B **54** 5326
[50] Durgun E, Ciraci S and Yildirim T 2008 Functionalization of carbon-based nanostructures with light transition-metal atoms for hydrogen storage *Phys. Rev.* B **77** 085405
[51] Nakada K and Ishii A 2011 Migration of adatom adsorption on graphene using DFT calculation *Solid State Commun.* **151** 13–6
[52] Ding Y and Wang Y 2018 Stable H-terminated edges, variable semiconducting properties, and solar cell applications of C_3N nanoribbons: a first-principles study *ACS Omega* **3** 8777–86
[53] Shi L B, Zhang Y Y, Xiu X M and Dong H K 2018 Structural characteristics and strain behaviors of two-dimensional C_3N: first principles calculations *Carbon* **134** 103–11
[54] Lee H, Choi W I, Nguyen M C, Cha M H, Moon E and Ihm J 2007 *Ab initio* study of dihydrogen binding in metal-decorated polyacetylene for hydrogen storage *Phys. Rev.* B **76** 195110
[55] Kubas G J 2001 Metal–dihydrogen and σ-bond coordination: the consummate extension of the Dewar–Chatt–Duncanson model for metal–olefin π bonding *J. Organomet. Chem.* **635** 37–68
[56] Züttel A 2003 Materials for hydrogen storage *Mater. Today* **6** 24–33
[57] Si L and Tang C 2017 The reversible hydrogen storage abilities of metal Na (Li, K, Ca, Mg Sc, Ti, Y) decorated all-boron cage B28 *Inter. J. Hydrogen Energy* **42** 16611–9
[58] Lide D R 1994 *Handbook of Chemistry and Physics* **75th** 864